Demonstration of a Closed-Loop Beam-Shaping System Based on the Phase-Only Carrier Method in High-Power Lasers

Beam-shaping applications in high-power laser systems have been presented in many different contexts such as the improvement of laser performance[1] or the manipulation of laser–target interactions.[2,3] These applications commonly employ static apodizers or deformable mirrors. Spatial-light modulators (SLM's) are also popular beam-shaping devices. Because of their low damage threshold and small aperture, they have been used in laser front ends[4] or inside laser cavities.[5] The advantage of SLM beam shapers lies in programmability and high spatial resolution, allowing for extremely fine control of the laser-beam profile. This is an especially important feature for maximizing the performance of high-power lasers. Defects or damages sites in the compressor gratings[6] or final optics assembly[7] often limit laser operation to a lower energy level. At the National Ignition Facility[8,9] efforts have been made to address this problem by introducing a programmable spot-shadowing system at an upstream image plane. An SLM-based beam-shaping system combined with closed-loop control has been recently demonstrated in a test-bed setup.[10,11] We have implemented this system in a multiterawatt laser[12] and at the front end of OMEGA EP's long-pulse beamlines.[13] This effort has revealed a few important issues that need to be addressed for applications in high-power laser systems. Among these, the problem of image distortion will be discussed here, followed by the problem of determining the damage threshold of an SLM device.

Previous work on adaptive beam shaping presented an algorithm based on direct linear mapping between the measured fluence and the command map of an SLM.[11] The motivation for direct mapping is to avoid characterizing the enormous number of influence functions associated with an SLM. A linear transformation is experimentally shown to be accurate enough for the imaging systems considered in high-power laser systems. Higher-order distortions such as barrel/pincushion distortions are negligible if the laser beams are image relayed with slow optics. On the other hand, image-distortion effects associated with the presence of tilted plates or wedges in the system are important for this application. As shown in Fig. 127.4, tilted plates/wedges introduce not only astigmatic image blurring[14] but also image shear. Such elements, e.g., beam diagnostic pickoffs, thin-film polarizers, or amplifier slabs, are ubiquitous in high-power lasers. The image shear can be represented as a linear transformation as follows:

$$\begin{pmatrix} x' \\ y' \end{pmatrix} = \begin{pmatrix} 1 & \sigma \\ 0 & 1 \end{pmatrix} \begin{pmatrix} x \\ y \end{pmatrix},$$

where σ is a shear parameter. This linear transformation can be combined with other linear transformations such as translation, magnification, and rotation. As a result, the sheared image can be numerically corrected. The transformation parameters are found by comparing a known phase or amplitude pattern introduced on the SLM and the measured pattern at the diagnostic image by running an optimization routine.

The blurring is caused by the axial astigmatism in the imaging system; i.e., the foci at sagittal and tangential planes are at different locations. Numerical simulations show that the severity of the blurring in the case of parallel plates is proportional to the tilt angle and the thickness of the plate. The wedged plate introduces an additional dependence of the blurring on the wedge angle and the distance from the image plane. Since the blurring limits the resolution of the beam profile to be shaped, it is best to design the optical system to minimize the axial astigmatism. It is possible to significantly reduce the effect by

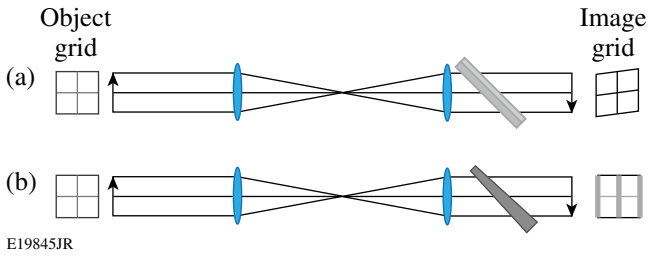

Figure 127.4
Arrangement of wedges and the effects on imaging. A rectangular grid is imaged by a 1-to-1 telescope, where a wedge is placed immediately behind the second lens. The affected image is shown on the right. (a) Image shear occurs when the wedge is placed vertically at an angle. (b) Image blurring occurs in one direction as indicated by the thicker vertical bars in the image grid.

using a compensator plate/wedge,[15] for example, a compensator wedge with the opposite angle.

A schematic of the experimental layout in a multiterawatt system[12] is shown in Fig. 127.5. The laser system is based on optical parametric chirped-pulse amplification (OPCPA) followed by a glass amplifier and compressor chamber. The closed-loop SLM beam-shaping system was implemented using two near-field image feedbacks, one (WFS1 in Fig. 127.5) placed nearby the SLM device and the other (WFS2 in Fig. 127.5) placed at the end of the system before the target chamber. The OPCPA laser beam is image relayed through the glass amplifier to the compressor chamber by three imaging telescopes. There are additional image relays on the diagnostic lines for WFS1 and WFS2 (in the dashed boxes).

The OPCPA front end produces 200-mJ pulses at 5 Hz. Only 10% of full OPCPA energy was used for this experiment and the glass amplifier was turned off. The SLM is an electrically addressed [liquid-crystal-on-silicon (LCOS)], nematic-type liquid crystal made by Hamamatsu. The SLM has 600×792 points, whereas the wavefront sensors have 130×130 sampling points. The wavefront sensors also provide near-field images with the same sampling as wavefront. The case of producing a flattop-profile laser beam was first demonstrated with WFS1. The diagnostic imaging system for WFS1 has a wedged leaky mirror that initially caused large spatial registration errors because of the image blurring. A secondary wedge compensator was inserted to restore the image quality. The result of flat-beam shaping is shown in Fig. 127.6. Within the flat area, the peak-to-mode improved from 39% to 12% and the relative rms (root mean square) improved from 9% to 3%.

Closed-loop control with WFS2 proved to be more difficult than with WFS1 because of the axial astigmatism in the system. The astigmatism comes not so much from the amplifier slabs because it is actually minimized by the orthogonal configuration of the slabs on the second pass of the beam. Ray tracing suggests that the astigmatism comes primarily from the compressor gratings. Calculations show that a 20-cm-thick, 1.5° wedge is needed as a compensator, which is not easily available. Therefore, the resolution of the calculated command map on the SLM was intentionally blurred to match the system resolution, which is necessary to prevent the ripple problem of the closed-loop control shaping.[11] The fluence distribution improved from 44% to 25% in peak-to-mode as shown in Figs. 127.7(a) and 127.7(b).

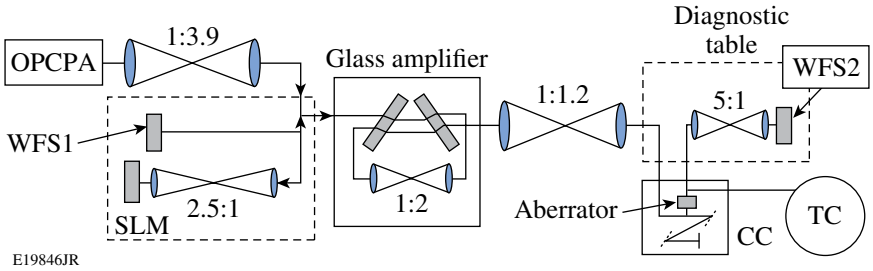

Figure 127.5
Experimental setup for demonstrating an SLM beam shaper in a multiterawatt laser system. CC: compressor chamber; TC: target chamber; WFS: wavefront sensor.

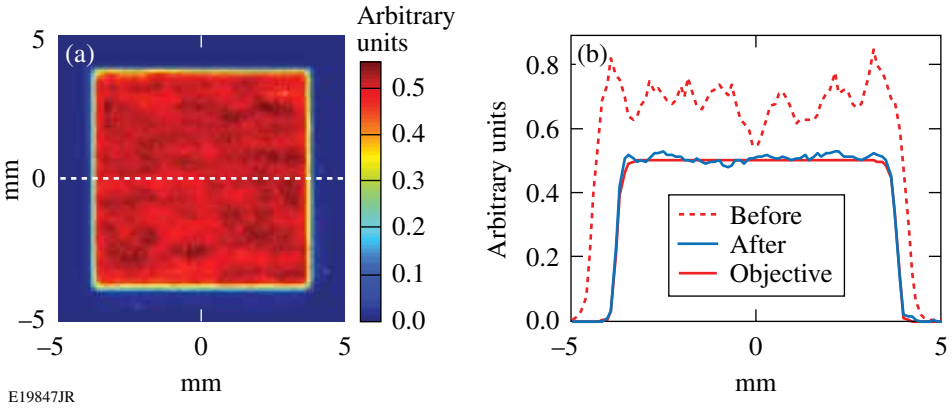

Figure 127.6
Flat-beam shaping with WFS1 (multiterawatt system). (a) Fluence after shaping; (b) fluence lineouts.

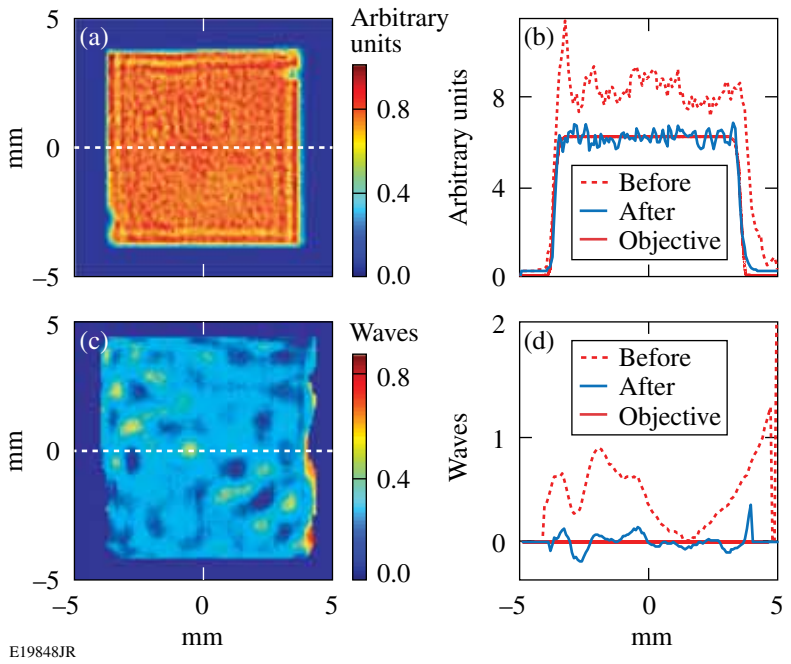

Figure 127.7
Beam-shaping results with WFS2 in the multiterawatt system. (a) Flat beam shaping; (b) lineout comparisons before and after beam shaping; (c) wavefront correction of aberrated beam; and (d) lineout comparison before and after wavefront correction.

The capability of high-order wavefront correction was tested in WFS2 closed-loop operation. A static wavefront aberrator was manufactured by the magnetorheological finishing process[12] using the map described in Ref. 11. Physical constraints prevented the phase plate from being placed exactly at the image plane of the SLM; therefore, the condition for closed-loop control was not optimum. Nevertheless, the rms value of the wavefront improved from 0.375 waves down to 0.08 waves [Figs. 127.7(c) and 127.7(d)].

The same beam-shaping system has been implemented in the front end of the OMEGA EP long-pulse beamlines. The initial application is to provide intensity smoothing of a beam, which is parabolically shaped by a static apodizer. The parabolic beam shape is used to precompensate for rod-amplifier–gain nonuniformity.[13] The test confirmed the effectiveness of the direct linear-mapping algorithm for intensity smoothing of a non-flat beam, as shown in Fig. 127.8. A comparable level of convergence error, 2% in relative rms, was achieved as in the OPCPA case. The image shear and rotation were numerically corrected.

Damage-threshold measurements over a small area (~500 μm) of an SLM sample with a focused beam resulted in varying values (from 570 mJ/cm^2 to 2 J/cm^2 over ten sites). This suggests that the damage-initiation sites or defects are sparsely distributed over the sample area. The measurement procedure is based on increasing the incident energy by a small step and waiting for a damage spot to occur for minutes of

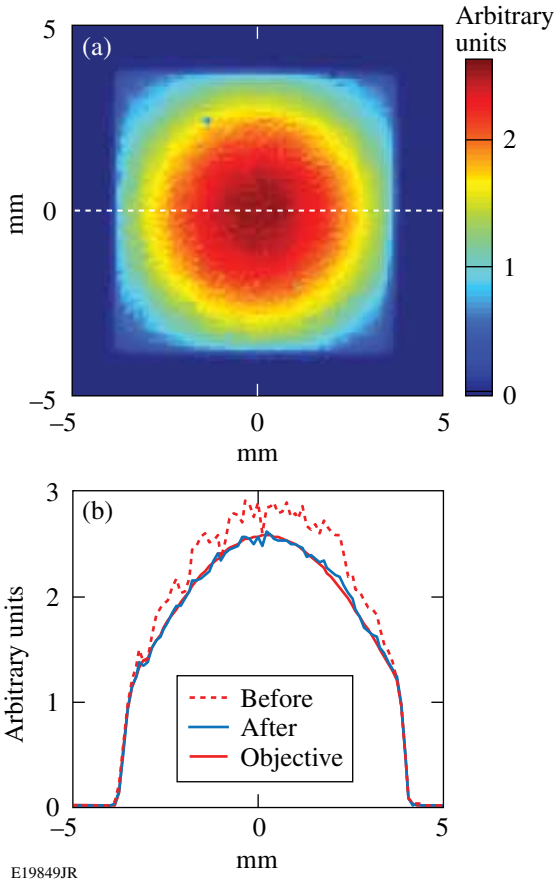

Figure 127.8
Parabolic beam shaping (OMEGA EP long-pulse front end). (a) Fluence after shaping; (b) fluence lineouts.

duration (a few thousand shots at 5 Hz). The energy is ramped up to the next level until damage is observed where the local fluence for the spot is estimated from the measured laser-beam profile. This procedure often takes several hours for a single site, so it is not practical to perform over hundreds of sites. We performed large-area (~5-mm) damage tests on samples that would effectively enable one to perform hundreds of small-area damage tests in a single ramp-up procedure. The samples were illuminated by 5-Hz, 2.5-ns laser pulses with an 8-mm × 8-mm square beam with a flattop profile. The laser pulses were generated from an optical-parametric conversion process at 1.053-μm wavelength. The laser energy on the sample was gradually increased, starting from 50 mJ to 100 mJ in 10-mJ steps. The duration of exposure at each step was 10 min or 3000 shots. The near-field image of the laser beam on the sample was measured every 10 s. The ramping and the short-term exposure continued until a damage site appeared on the near-field image. The local damage fluence at the damage site was calculated based on the separate incident-energy measurement and the calibrated near-field image. The calculated local fluences at the observed damaged sites of the three samples (two of them being under active condition) were 230, 235, and 267 mJ/cm^2. The minimum of these values can be considered as the damage-threshold fluence. Considering the use area of the SLM to be ~1 cm^2 within a 12 × 16-mm^2 total area of the actual device, the total energy the SLM can handle is ~230 mJ. The safe energy level can be much lower than this, depending on the local beam modulation of the incident beam.

A successful closed-loop beam shaping was demonstrated in a multiterawatt laser and in an OMEGA EP long-pulse front end. The main issues of implementing an LCOS-SLM beam-shaping system in high-power laser systems have been discussed. It was demonstrated that the imaging-registration problems can be either numerically corrected or avoided by design. The damage threshold of SLM's can be measured by the method described here to ensure safe operations in high-power laser systems. One of the future challenges will be to develop a larger-area or a higher-damage-threshold SLM to accommodate higher-energy operation.

ACKNOWLEDGMENT

This work was supported by the U.S. Department of Energy Office of Inertial Confinement Fusion under Cooperative Agreement No. DE-FC52-08NA28302, the University of Rochester, and the New York State Energy Research and Development Authority. The support of DOE does not constitute an endorsement by DOE of the views expressed in this article.

REFERENCES

1. C. Dorrer, Opt. Lett. **34**, 2330 (2009).
2. B. Wattellier *et al.*, J. Opt. Soc. Am. B **20**, 1632 (2003).
3. O. Boyko *et al.*, Opt. Commun. **246**, 131 (2005).
4. N. Sanner *et al.*, in *Conference on Lasers and Electro-Optics* (Optical Society of America, Washington, DC, 2004), Vol. 1, Paper CTuP34.
5. J. Bourderionnet *et al.*, Opt. Lett. **26**, 1958 (2001).
6. J. Qiao, A. W. Schmid, L. J. Waxer, T. Nguyen, J. Bunkenburg, C. Kingsley, A. Kozlov, and D. Weiner, presented at the 2010 International Committee on Ultra-High Intensity Lasers Conference, Watkins Glen, NY, 26 September–1 October 2010 (Paper FO3).
7. A. Conder *et al.*, in *Laser-Induced Damage in Optical Materials: 2007*, edited by G. J. Exarhos *et al.* (SPIE, Bellingham, WA, 2007), Vol. 6720, p. 672010.
8. S.-W. Bahk, J. D. Zuegel, J. R. Fienup, C. C. Widmayer, and J. Heebner, Appl. Opt. **47**, 6586 (2008).
9. J. Heebner *et al.*, in *Laser-Induced Damage in Optical Materials: 2010*, edited by G. J. Exarhos *et al.* (SPIE, Bellingham, WA, 2010), Vol. 7842, p. 78421C.
10. V. Bagnoud and J. D. Zuegel, Opt. Lett. **29**, 295 (2004).
11. S.-W. Bahk, E. Fess, B. E. Kruschwitz, and J. D. Zuegel, Opt. Express **18**, 9151 (2010).
12. V. Bagnoud, M. J. Guardalben, J. Puth, J. D. Zuegel, T. Mooney, and P. Dumas, Appl. Opt. **44**, 282 (2005).
13. M. J. Guardalben and L. J. Waxer, in *High Power Lasers for Fusion Research*, edited by A. A. S. Awwal, A. M. Dunne, H. Azechi, and B. E. Kruschwitz (SPIE, Bellingham, WA, 2011), Vol. 7916, Paper 79160G.
14. R. Korniski and J. K. Lawson, in *International Optical Design Conference*, 2002 OSA Technical Digest Series (Optical Society of America, Washington, DC, 2002), Paper ITuD5.
15. J. W. Howard, Appl. Opt. **24**, 4265 (1985).